

## Velocity Oscillations in Microfluidic Flows of Concentrated Colloidal Suspensions

Lucio Isa, Rut Besseling, Alexander N. Morozov, and Wilson C. K. Poon

*SUPA, School of Physics & Astronomy, The University of Edinburgh, James Clerk Maxwell Building,  
The Kings Buildings, Mayfield Road, Edinburgh EH9 3JZ, United Kingdom*

(Received 27 June 2008; published 4 February 2009)

We study the pressure-driven flow of concentrated colloids confined in glass microchannels at the single-particle level using fast confocal microscopy. For channel to particle size ratios  $2a/\bar{D} \lesssim 30$ , the flow rate of the suspended particles shows fluctuations. These turn into regular oscillations for higher confinements ( $2a/\bar{D} \approx 20$ ). We present evidence to link these oscillations with the relative flow of solvent and particles (permeation) and the effect of confinement on shear thickening.

DOI: [10.1103/PhysRevLett.102.058302](https://doi.org/10.1103/PhysRevLett.102.058302)

PACS numbers: 83.80.Hj, 83.50.-v, 83.60.Rs, 83.60.Wc

The bulk flow of colloidal suspensions has long been a subject for investigation [1]. Nowadays, the availability of micro- and nanofluidic devices [2] also necessitates the understanding of flows in confined geometries. Confinement effects are inevitable when colloids are transported through structures with dimensions  $\lesssim 10^2$  particle diameters. Thus, such effects occur when colloidal inks flow through micronozzles [3–5], and must be important in the transport of particles through lipid nanotubes [6].

The study of confined colloidal flow may also have wider implications. First, some aspects of the flow of suspensions may usefully be compared to that of dry granular matter [7,8] and dense emulsions [9], so that fruitful comparison may extend to confined flows. Second, it has recently become possible to pump atomic and molecular liquids through carbon nanotubes and similar structures [10]. Since excluded volume effects between molecules are strong in such liquids if hydrogen bonding is absent, the study of confined colloidal flow may provide significant insight: such “knowledge transfer” from the colloidal to the atomic and molecular domain is already well established in the study of equilibrium phenomena [11], including the structural effects of confinement [12].

In this Letter, we use real-time single-particle imaging [13] to study confinement in the simplest possible concentrated colloid, a suspension of hard spheres, flowing in one of the simplest possible geometries, a square channel. The motivation for studying such a well-characterized model system is twofold. First, excluded volume effects between particles are hard to “turn off,” so that phenomena discovered in our system are likely generic. Second, data from a well-characterized system should allow direct comparison with future theories. We observe confinement-induced flow instabilities, in the form of large-amplitude oscillations. We propose that these oscillations are an unexpected and dramatic consequence of the recently discovered effect of confinement on shear thickening [14]. The ubiquity of the latter phenomenon in colloid rheology [1] suggests that the instability we observed may also occur widely.

We used sterically stabilized polymethylmethacrylate (PMMA) spheres (diameter  $\bar{D} = 2.6 \pm 0.1 \mu\text{m}$ , volume

fraction  $\Phi \geq 0.63$ , from confocal microscopy, Brownian time  $\tau_B = 4.4 \text{ s}$ ), fluorescently labeled with nitrobenzoxadiazole and suspended in a mixture of cycloheptylbromide and mixed decalin (viscosity  $2.6 \text{ mPa s}$ ) for buoyancy matching at room temperature. A pressure difference,  $\Delta P$  ( $\approx 10^2$  to  $10^4 \text{ Pa}$ , see [15] for details), is applied to drive the suspension into square borosilicate glass microchannels (Vitrocom, Ltd.; width  $2a = 50, 80, \text{ and } 100 \mu\text{m}$ ) with untreated, smooth inner walls. The channel dimensions ( $2a/\bar{D} \approx 20, 30 \text{ and } 40$ ) were not integral multiples of  $\bar{D}$  to avoid complete layering.

The flow across the full width of the channel  $y$  was imaged with a Visitech VTeye confocal scanner and a Nikon TE 300 inverted microscope. We collected  $44 \mu\text{m} \times 58 \mu\text{m}$  images (107 frames/s) at  $17 \mu\text{m}$  from the lower surface. From these we located (resolution  $\approx 50 \text{ nm}$ ) and tracked particles [13,16]. From the single-particle velocities we calculated the macroscopic flow velocity, averaged over five frames to eliminate high frequency instrumental and tracking noise.

In the widest channel ( $2a/\bar{D} \approx 40$ ), the velocity is steady with time, Fig. 1(c) [17]. The velocity profile and density (data not shown) do not vary with position along the channel  $x$  after entrance effects. The velocity profile consists of shear zones near the walls and a central plug with a flow-speed-independent size. We have recently shown that such profiles can be understood using a model developed for granular pipe flow [7].

The situation is radically transformed when the channel size is halved (to  $2a/\bar{D} \approx 20$ ). The average velocity profile and density are now  $x$  dependent, Fig. 1(a). Near the inlet ( $x = 0$ ) we find the same kind of sheared profile as in the wider channels. Further downstream we encounter another region where the central plug extends across the full channel; i.e., the shear between particles is completely absent and the suspension flows as a solid body with velocity  $V$ ; in this complete plug region the density reaches a maximum value  $\Phi_p$ , and remains constant over  $\sim 1 \text{ cm}$  ( $\sim 4000\bar{D}$ ), before terminating even further downstream at a sharp interface with another sheared region, Fig. 1(a), whose density decreases away from the plug. Dramatic, quasire-

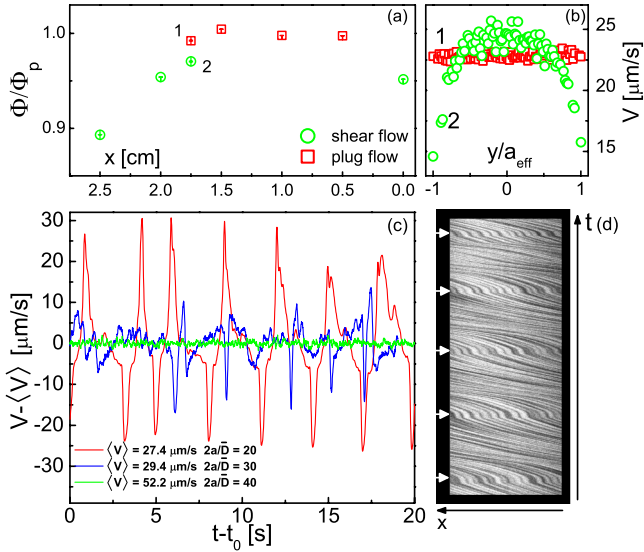


FIG. 1 (color online). (a) Normalized particle volume fraction as a function of  $x$  from particle counting in 1000 frames. (b) Velocity profiles as a function of normalized  $y$  ( $a_{\text{eff}} = a - \bar{D}/2$ ) corresponding to points 1 and 2 in (a). (c) Velocity offset by the long-time average as a function of time for three different channel sizes. (d) Space-time ( $x$ - $t$ ) diagram of oscillating flow in a  $\approx 20\bar{D}$  channel. The arrows highlight jamming events.

gular velocity oscillations are also seen, Fig. 1(c). The oscillations are lower in amplitude and less regular in a  $\approx 30\bar{D}$  channel, and absent when the channel is widened to  $\approx 40\bar{D}$ .

Figure 1(d) shows a “space-time diagram” of the oscillations in the  $\approx 20\bar{D}$  channel, constructed by stacking one-pixel-wide  $y$  bins taken from consecutive images in the channel’s center, in the region of complete plug flow. Changes in the slope of the traces correspond to changes in the flow speed, and we observe regularly spaced horizontal bands corresponding to events where the flow jams and comes to an almost complete arrest.

These regular jams are absent below a particular threshold driving pressure, corresponding to a threshold average flow rate  $V_{\text{thr}}$ . In a typical experiment, Fig. 2, an initial small driving pressure  $\Delta P_0$  is applied and then stepped up

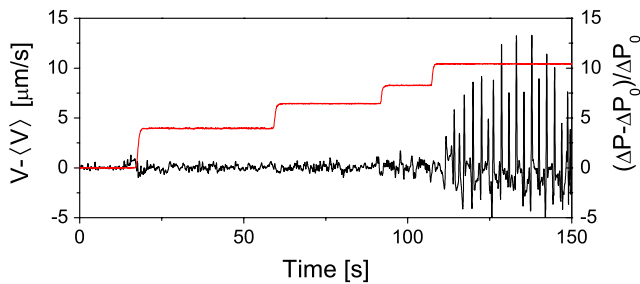


FIG. 2 (color online). Flow velocity  $V(t)$  (black, left axis), offset by the long-time average  $\langle V \rangle$  ( $2a \approx 20\bar{D}$ ). Right axis (red or gray): corresponding driving pressure  $\Delta P$  normalized by the initial  $\Delta P_0$ . During each pressure step,  $\Delta P$  is a constant.

taking the flow into an oscillatory regime. Flow rate oscillations and nonuniform density along the flow make it unfeasible to access the local pressure from the macroscopic  $\Delta P$ . Moreover, the relation between applied  $\Delta P$  and measured  $\langle V \rangle$  can be strongly history dependent. Therefore the following discussion is performed in terms of the flow rate, which constitutes the relevant local, measured control parameter.

To emphasize the highly regular nature of the oscillations observed in  $\approx 20\bar{D}$  channels, we show in Fig. 3 their power spectrum. Superposing the fundamental frequency and the first five harmonics reproduces the gross features of the velocity wave form (inset, Fig. 3). We measured the fundamental frequency of the oscillations as a function of the local average speed  $\langle V \rangle$ , Fig. 4. The flow is steady for average velocities below a run-dependent threshold, while oscillations arise above this threshold (bottom inset, Fig. 4). The fundamental frequency  $f$  can be fitted by  $f(\langle V \rangle) = \alpha(\langle V \rangle - V_{\text{thr}})^\beta$ , where  $f$  extrapolates to 0 at  $V_{\text{thr}}$  (for the curve in the inset  $V_{\text{thr}} = 10.06 \mu\text{m/s}$ ) and  $\alpha$  and  $\beta$  are fitting parameters. Plotting  $f$  versus  $\langle V \rangle - V_{\text{thr}}$  collapses all the data onto one single curve, which is fitted by a power law with exponent  $\beta = 0.34 \pm 0.13$ .

The amplitude of the oscillations (quantified by the standard deviation of the velocity signal, Fig. 4, top inset) shows a linear increase with flow speed above the threshold. The offset for  $\langle V \rangle - V_{\text{thr}} = 0$  represents the upper limit of the noise in nonoscillating signals. This linear dependence is directly related to the fact that at each jamming event, the velocity drops from roughly  $\approx \langle V \rangle$  to a much lower value that is only weakly dependent on the average flow speed.

Interestingly, although the oscillations become less regular when we widened the channel to  $\approx 30\bar{D}$ , Fig. 1, the fundamental frequency and its dependence on flow speed hardly differ from what we measured for  $\approx 20\bar{D}$  channels, Fig. 4. This observation, together with the fact that our sampling frequency is 2 to 3 orders of magnitude higher than the frequencies reported in Fig. 4, confirm that

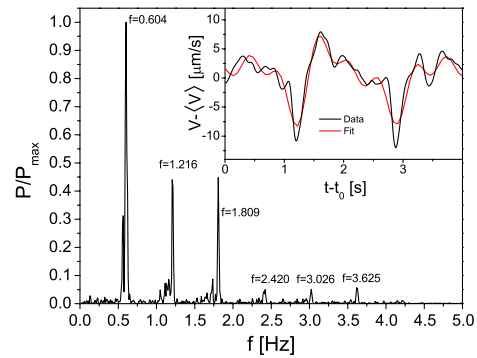


FIG. 3 (color online). Normalized power spectrum of an oscillating velocity signal in a  $\approx 20\bar{D}$  channel ( $\langle V \rangle = 20.4 \mu\text{m/s}$ ). Inset: 4 secs. of the offset velocity signal with the fit obtained from the superposition of 6 sine waves from the power spectrum (red or gray).

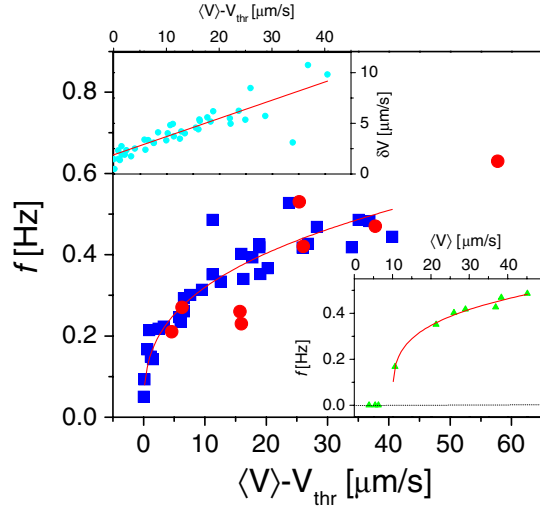


FIG. 4 (color online). Fundamental frequency of the velocity oscillations as a function of  $\langle V \rangle - V_{thr}$  ( $\square \approx 20\bar{D}$ ,  $\bullet \approx 30\bar{D}$ ); the full curve is a power-law fit with exponent  $0.34 \pm 0.13$ . Top inset: amplitude (standard deviation) of the velocity oscillations vs  $\langle V \rangle - V_{thr}$  (points) and a linear fit (line). Bottom inset: fundamental oscillations frequency  $f$  vs the average flow speed  $\langle V \rangle$  for one run (points) with a power-law fit (curve).

the absence of oscillations in the  $\approx 40\bar{D}$  channels is not an artifact due to experimental limitations.

Summarizing our observations, we find that under strong confinement (channel width  $2a/\bar{D} \approx 20$ ) and above a threshold flow rate, the flow velocity oscillates while driven by a constant pressure difference. The frequency and the amplitude of the oscillations increase with flow rate. The velocity profile and particle density are nonuniform along the channel. Increasing the channel width to  $2a/\bar{D} \approx 30$  leads to lower amplitude, less regular oscillations, but the threshold flow rate and oscillation frequencies are little changed. The velocity oscillations and spatial nonuniformities along the flow direction completely disappear when the channel width is doubled ( $2a/\bar{D} \approx 40$ ).

We do not yet have a quantitative theory of these confinement-driven flow instabilities. Qualitatively, however, we propose that the phenomenon results from the interplay between permeation [18] and strong shear thickening [14]. When the suspension is momentarily jammed (time point 1 in the  $\langle V(t) \rangle$  plot in Fig. 5) the applied pressure gradient still drives solvent flow through the stationary plug of particles. This permeation flow erodes particles from the front of the plug, forming a lower density region. A rarefaction wave propagates upstream, unjamming the plug (time point 2, Fig. 5). At the same time, the lower density region at the front can sustain shear. Above a threshold flow rate, which we estimate to be  $Pe \approx 2$ , this region can exhibit strong jamming, akin to transient shear thickening [19]. As the sheared front thickens, it slows down, and particles accumulate upstream, increasing the local density and enhancing the tendency to shear thicken, until the front once more jams suddenly (time point 3,

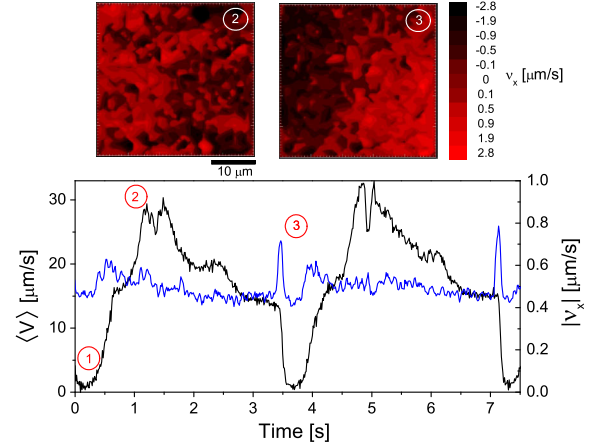


FIG. 5 (color online). Plug velocity  $\langle V(t) \rangle$  in the lab frame (left axis, black curve) and absolute value of the  $x$  component of particle velocities in the CM frame  $|\nu_x(t)|$ . The values of  $\nu_x$  have been calculated using particle displacements over 0.1 s. Top: spatial distributions of  $\nu_x$  over the field of view. Positive flow direction from right to left.

Fig. 5) [20]. A compaction wave passes upstream, and the cycle repeats. Crucially, Fall *et al.* [14] recently reported that the tendency to shear thicken was enhanced under confinement. This may explain why we only observe instabilities in narrow enough channels.

Evidence for a lower density, sheared region at the front has already been shown in Fig. 1. Detailed analysis of single-particle data provides evidence for the rarefaction and compression waves. We were unable to observe these very small density changes directly, but have been able to deduce their presence by examining particle displacements in the plug's comoving (CM) frame. Figure 5 reports the absolute value of the  $x$  component of the particle velocity in this frame,  $|\nu_x|$  (blue curve), as well as the plug velocity in the lab frame,  $\langle V \rangle$  (black curve), over two cycles of oscillations. The sum of the signed values  $\nu_x$  is zero in the CM frame by definition, while peaks in  $|\nu_x|$  evidence additional relative motion between the particles. We indeed observe a rises in  $|\nu_x|$  as the plug successively unjams (time point 1) and jams (time point 3). Spatial maps of the signs of  $\nu_x$  (top of Fig. 5) confirm that these are rarefaction and compaction waves, respectively.

In our scenario, the frequency of the oscillations is probably controlled by the need for the sheared region to accumulate a finite strain before jamming takes place. Multiplying the local shear rate in front of the plug (extracted from the velocity profiles) and the inverse frequency of the oscillations yields a value of 2 to 10, weakly dependent on  $\langle V \rangle$ . This suggests analogies with strain thickening in concentrated colloids [22].

Further insight into our proposed mechanism comes from examining the transition region from plug to shear flow. Particle trajectories from this region, Fig. 6, clearly show that the flow here is convergent. Such convergent flow is reminiscent of behavior at an imposed geometrical

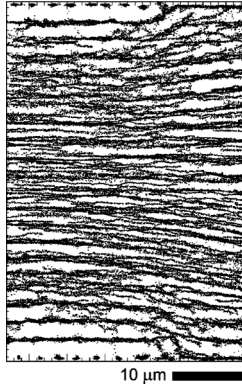


FIG. 6. Left: superposition of particles positions during flow (right to left,  $\langle V \rangle \approx 25 \mu\text{m/s}$ , 50 images) at the plug-shear interface showing converging streamlines.

constriction. Indeed, intermittent jamming was observed at the inlet of the flow of concentrated hard-sphere colloids into a narrow capillary [23]. Similar phenomena are also well known in granular materials (e.g., the hourglass [24]). There is, however, an important difference in our case, Fig. 6: here, the “constriction” into which some of the particles flow convergently is due to a self-organized configuration of other particles.

Recall that in  $\approx 20\bar{D}$  and  $\approx 30\bar{D}$  channels, we see longitudinal inhomogeneities, and therefore associated “self-organized” convergent flows at the “plug-shear” interface, at all flow speeds, although oscillations emerge only when the flow speed is high enough, presumably because high speeds are needed to jam the convergent flow. These considerations also suggest that the details of confinement-induced shear thickening in our system differ from the system studied by Fall *et al.* [14]. Significantly, we never observed any longitudinal inhomogeneities in  $\approx 40\bar{D}$  channels, and hence no plug-shear interface or self-organized convergent flows. This suggests that our failure to observe oscillations in these wider channels is not because we did not reach high enough flow speeds; rather, the flow instability described here is an intrinsic confinement effect.

To conclude, we explore the wider relevance of our observation of confinement-induced oscillations in the flow of concentrated hard-sphere suspensions. First, we note that oscillations are in fact ubiquitous in the pipe flow of pastes. Interestingly, if the pipe diameter is expressed in units of average particle diameter, a number of previous studies of oscillations in paste flow clearly overlap or just border the regime we have explored (e.g.,  $\sim 10\text{--}40\bar{D}$  in [18] and  $\sim 50\text{--}100\bar{D}$  in [25]). While previous research has noted the importance of permeation and inhomogeneities along the flow direction [18], the role of confinement was not considered. Previous studies typically used much bigger particles and therefore worked at significantly higher Pe than in the present investigation; nevertheless, our results do suggest that confinement can-

not safely be neglected. Second, we point out that the strong confinement effects we observe recall analogies in dry granular flow [24,26,27]. Interestingly, in place of the solvent permeation that is important in our experiments, air flow can play a crucial role in confinement-driven granular oscillations [24]. Finally, the occurrence of instabilities in flowing colloids under confinement must be taken into account in microfluidic applications [2,5].

We thank A. B. Schofield for synthesizing PMMA particles and M. E. Cates for illuminating discussions. L. I. was funded by the EU network MRTN-CT-2003-504712. The EPSRC funded R. B. (GR/S10377 & EP/D067650) and W. C. K. P. (EP/D071070). A. N. M. thanks the RSE/BP Trust for financial support.

- [1] R. G. Larson, *The Structure and Rheology of Complex Fluids* (Oxford University Press, Oxford, 1999).
- [2] D. Psaltis *et al.*, *Nature (London)* **442**, 381 (2006).
- [3] J. A. Lewis, *Curr. Opin. Solid State Mater. Sci.* **6**, 245 (2002).
- [4] S. Michna *et al.*, *Biomaterials* **26**, 5632 (2005).
- [5] M. T. Roberts *et al.*, *Langmuir* **23**, 8726 (2007).
- [6] R. Karlsson *et al.*, *Langmuir* **18**, 4186 (2002).
- [7] L. Isa *et al.*, *Phys. Rev. Lett.* **98**, 198305 (2007).
- [8] T. L. Pennec *et al.*, *Phys. Fluids* **10**, 3072 (1998).
- [9] J. Goyon *et al.*, *Nature (London)* **454**, 84 (2008).
- [10] D. Mattia and Y. Gogotsi, *Microfluid. Nanofluid.* **5**, 289 (2008).
- [11] W. C. K. Poon, *Science* **304**, 830 (2004).
- [12] K. Binder, *Annu. Rev. Mater. Res.* **38**, 123 (2008).
- [13] R. Besseling, L. Isa, E. R. Weeks, and W. C. K. Poon, *Adv. Colloid Interface Sci.* (to be published).
- [14] A. Fall *et al.*, *Phys. Rev. Lett.* **100**, 018301 (2008).
- [15] L. Isa *et al.*, *J. Phys. Conf. Ser.* **40**, 124 (2006).
- [16] J. C. Crocker and D. G. Grier, *J. Colloid Interface Sci.* **179**, 298 (1996).
- [17] We report the flow velocity  $V$  offset by the long-time average  $\langle V \rangle$ , where the latter is calculated on windows 2–3 times larger than the typical oscillation periods.
- [18] P. Yaras *et al.*, *Rheol. Acta* **33**, 48 (1994).
- [19] We found by cone-plate rheometry (cone radius 2 cm, angle  $1^\circ$ , truncation gap  $30 \mu\text{m}$ ) that  $\bar{D} = 1.3 \mu\text{m}$  particles showed shear thickening for  $0.5 \leq \text{Pe} \leq 5$  at  $\Phi \approx 0.6$ , comparable to conditions in the sheared zone in front of the plug.
- [20] Interestingly, dense suspensions are known to exhibit quasiregular giant stress oscillations near the jamming transition [21].
- [21] D. Lootens, H. van Damme, and P. Hébraud, *Phys. Rev. Lett.* **90**, 178301 (2003).
- [22] J. R. Melrose and R. C. Ball, *J. Rheol. (N.Y.)* **48**, 961 (2004).
- [23] M. D. Haw, *Phys. Rev. Lett.* **92**, 185506 (2004).
- [24] X.-L. Wu *et al.*, *Phys. Rev. Lett.* **71**, 1363 (1993).
- [25] R. B. Lukner and R. T. Bonnecaze, *J. Rheol. (N.Y.)* **43**, 735 (1999).
- [26] J.-C. Tsai *et al.*, *Phys. Rev. E* **65**, 011306 (2001).
- [27] S. Horluck *et al.*, *Phys. Rev. E* **67**, 021304 (2003).